Volume 4 | Number 2 | February 2014 | Pages 247–570

Catalysis Science & Technology

www.rsc.org/catalysis

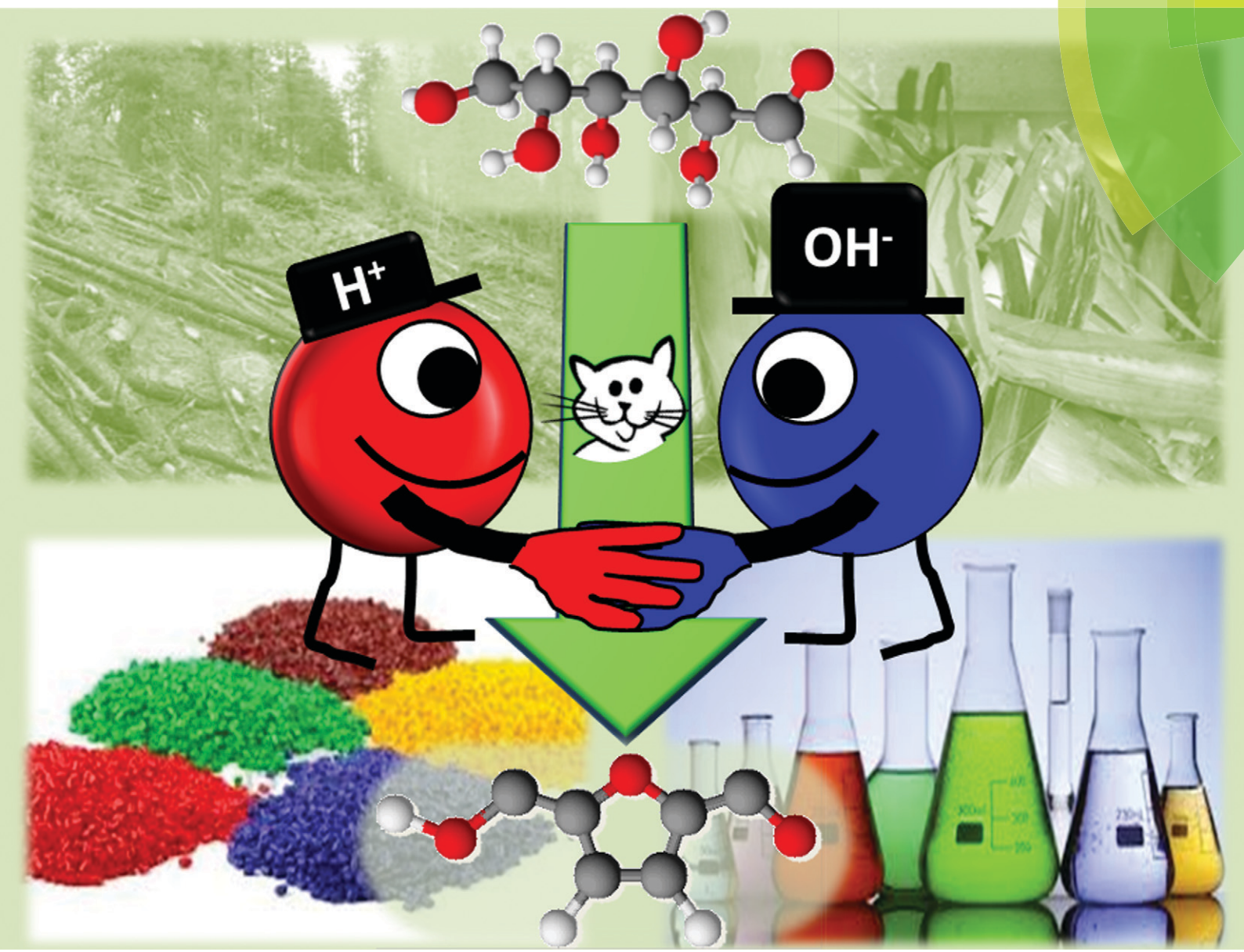

ISSN 2044-4753

ROYAL SOCIETY OF CHEMISTRY

COVER ARTICLE
Wilson *et al.*
Bifunctional SO_4/ZrO_2 catalysts for 5-hydroxymethylfufural (5-HMF) production from glucose

Catalysis Science & Technology

PAPER

View Article Online
View Journal | View Issue

Cite this: *Catal. Sci. Technol.*, 2014, 4, 333

Bifunctional SO_4/ZrO_2 catalysts for 5-hydroxymethylfufural (5-HMF) production from glucose†

Amin Osatiashtiani,[ab] Adam F. Lee,[bc] D. Robert Brown,[d] Juan A. Melero,[e] Gabriel Morales[e] and Karen Wilson*[ab]

Received 15th June 2013,
Accepted 5th August 2013

DOI: 10.1039/c3cy00409k

www.rsc.org/catalysis

The telescopic conversion of glucose to fructose and then 5-hydroxymethylfurfural (5-HMF), the latter a potential, bio-derived platform chemical feedstock, has been explored over a family of bifunctional sulfated zirconia catalysts possessing tuneable acid–base properties. Characterisation by acid–base titration, XPS, XRD and Raman reveal that submonolayer SO_4 coverages offer the ideal balance of basic and Lewis–Brønsted acid sites required to respectively isomerise glucose to fructose, and subsequently dehydrate fructose to 5-HMF. A constant acid site normalised turnover frequency is observed for fructose dehydration to 5-HMF, confirming a common Brønsted acid site is responsible for this transformation.

Introduction

Concern over dwindling fossil fuel reserves, and the impact of CO_2 emissions on climate change, is driving the quest for alternative feedstocks to reduce dependence on non-renewable sources of fuels and chemicals. Biomass offers the only renewable source of organic molecules for the manufacture of bulk, fine and speciality chemicals necessary to secure the future needs of society. To be sustainable, so called 'second generation' biomass feedstocks must be sourced from non-edible components of crops (such as stems, leaves and husks), cellulose from agricultural or forestry waste, or high yielding short rotation non-food crops such as Switch grass or Willow which require minimal cultivation. While such lignocellulosic materials are attractive feedstocks for both fuel and chemical production *via* bio- or thermochemical platforms,[1,2] significant catalyst development is essential to improve the efficiency with which biomass derived building blocks can be processed. Specifically, new methods are required to selectively *deoxygenate* the highly functional molecules obtained from cellulose, contrasting with historic selective *oxygenation* routes developed for petroleum feedstocks.

In 2004, the US DoE identified a range of sugar-derived platform chemicals obtainable *via* chemical or biochemical transformation of lignocellulosic biomass,[3] subsequently revisited by Bozell and Petersen in 2010.[4] Furanic components such as 5-hydroxymethylfurfural (5-HMF) and furfural were identified as key chemical intermediates that can be synthesised from sugars.[5] Potential applications include the production of linear alkanes of the molecular weight desired for transformation into diesel and jet liquid fuels, with 5-HMF also a precursor to valuable chemical building blocks such as levulinic acid, 2,5-furandicarboxylic acid (FDA), 2,5-diformylfuran (DFF), dihydroxymethylfuran and 5-hydroxy-4-keto-2-pentenoic acid for the synthesis of diverse polymers and plastics.[6] Conversion of C_6 sugars to 5-HMF is of significant current interest, with liquid mineral acids including H_2SO_4, HCl and H_3PO_4 frequently employed to catalyse the necessary dehydration. However, commercial implementation of 5-HMF as a chemical intermediate is impeded by high production costs.[7] A heterogeneously catalysed route to directly convert glucose into 5-HMF in aqueous media thus remains highly sought after. Most research has focused on the more facile conversion of fructose (as a model saccharide) to 5-HMF,[8–18] to circumvent the formation of side products such as oligosaccharides and humins[19] commonly reported during acid catalysed glucose conversion. Many studies have also resorted to non-aqueous solvents in an effort to improve overall 5-HMF yield. While high 5-HMF yields are reported following fructose dehydration in dimethyl sulfoxide

[a] *Present Address: European Bioenergy Research Institute, School of Engineering and Applied Sciences, Aston University, Aston Triangle, Birmingham, B4 7ET, UK. E-mail: k.wilson@aston.ac.uk*
[b] *School of Chemistry, Cardiff University, Main Building, Cardiff, CF10 3AT, UK. E-mail: OsatiashtianiA@cardiff.ac.uk*
[c] *Present Address: Department of Chemistry, University of Warwick, Coventry, CV4 7AL, UKSchool of Chemistry, Monash University, Victoria 3800, Australia. E-mail: A.F.Lee@warwick.ac.uk*
[d] *School of Applied Sciences, University of Huddersfield, Huddersfield, HD1 3DH, UK. E-mail: d.r.brown@hud.ac.uk; Tel: 01484 473397*
[e] *Department of Chemical & Environmental Technology, Universidad Rey Juan Carlos, C/Tulipan. s/n. E-28933, Móstoles, Madrid, Spain. E-mail: juan.melero@urjc.es; Fax: +34 91-488-74-68*

† Electronic Supplementary Information (ESI) available: Porosimetry, tables of product data from catalytic reactions. See DOI: 10.1039/c3cy00409k

(DMSO)[16] due to the aprotic solvent inhibiting levulinic acid and humin formation,[20] product separation is problematic due to the formation of toxic sulfur compounds during high temperature DMSO distillation.[21] Ionic liquids are an attractive processing solvent for carbohydrates; partnership with a homogeneous metal halide catalyst offers 5-HMF yields from glucose of ~70%, however separation and catalyst recovery issues remain.[22]

Since biomass pre-treatment, such as steam explosion[23] or enzymatic[24] and chemical (acid or base)[25,26] promoted cellulose hydrolysis, will ultimately produce aqueous sugar sources, routes to convert the cheaper and more abundant glucose to 5-HMF in water remain a challenge. Operation in biphasic systems (*e.g.* water/MIBK), which allows reactive extraction of 5-HMF from the aqueous phase thereby limiting side reactions, is a promising approach to continuous 5-HMF production,[8,27] when catalysed by liquid[8,28,29] or solid acids.[30–32] A tandem homogeneous Lewis/Brønsted acid catalysed process, utilising $AlCl_3$ and HCl in a biphasic system of water/2-*sec*-butylphenol to respectively isomerise glucose to fructose and then dehydrate fructose to 5-HMF, recently achieved a 62% 5-HMF yield.[33] Other homogeneous metal halides,[34,35] including Cr(III) Zn(II) and Sn(IV) and more water tolerant lanthanide chloride,[36] can also effect glucose conversion, but confer lower HMF selectivity of ~45–48%. In practice, the use of soluble catalysts, particularly $AlCl_3$ (which reacts violently with water), remains a concern due to the associated toxic waste levels that could result from scaled-up processes, and thus at odds with Green Chemistry principles. The application of Lewis acidic Sn-β zeolite in conjunction with aqueous HCl can convert glucose to 5-HMF in a biphasic system at 180 °C with ~60% HMF selectivity, however the use of corrosive HCl remains undesirable.[37] A tandem reaction using solid base hydrotalcites and solid acid resins in a single reactor is most promising, although reaction was conducted in *N*,*N*-dimethylformamide instead of water.[38] Practical and efficient glucose to 5-HMF conversion thus awaits improved bi-functional solid acid and base catalysts which can operate in the aqueous phase. In this regard, progress has been unfortunately hampered by a lack of detailed analysis including mass balances, and systematic studies correlating catalyst acid–base properties with performance.

The amphoteric properties of zirconia make it an attractive catalytic material to employ in such a bi-functional process.[39,40] Indeed zirconia has been reported as a catalyst for the isomerisation of glucose to fructose at 200 °C,[41] while sulfated zirconia (SZ) is also an attractive strong solid acid for alcohol dehydration. Initial reports relating to the performance of SZ in aqueous phase catalysis are somewhat disappointing, reflecting instability under high temperature hydrothermal conditions, most likely associated with dissolution of multilayer sulfate species present at the high S contents employed.[16,42] The potential for tuning the acid strength in SO_4/ZrO_2 and thereby imparting bi-functionality at low sulfate contents for glucose conversion has been neglected to date. Our previous work showed that the acid strength of SZ can be readily tuned to direct selectivity in liquid phase terpene isomerisation.[43] We thus hypothesised that judicious control over sulfur loading content may enable predictable tuning of the one-pot conversion of glucose to 5-HMF, by optimising the relative surface coverage of sulfate acid and ZrO_2 base sites arising from the parent support. Here we demonstrate that systematic control over the Lewis–Brønsted acid and base properties of SZ enables the telescopic isomerisation of glucose to fructose, and subsequent fructose dehydration to 5-HMF in aqueous media, employing a single bi-functional heterogeneous catalyst.

Experimental

Catalyst preparation

A series of SZ catalysts with different SO_4^{2-} loadings were prepared by impregnation of 50 g $Zr(OH)_4$ (MEL Chemicals – XZO 880/01) with 500 ml $H_2SO_{4(aq)}$ of molarity 0.01–0.5 M. The slurry was stirred for 5 h at ambient temperature, filtered and dried at 80 °C overnight, and then calcined at 550 °C for 3 h. Catalysts were stored in air and used without pre-treatment.

Catalyst characterisation

Surface area and pore size analysis was performed by N_2 physisorption on a Quantasorb Nova 2000 instrument, after sample out gassing at 120 °C for 2 h. Surface areas were calculated using the Brunauer–Emmett–Teller (BET) method over the range P/P_0 = 0.03–0.18, where a linear relationship was maintained. Pore size distributions were calculated using the Barrett–Joyner–Halenda (BJH) model applied to the desorption branch of the isotherm. Bulk S contents were determined by EDX employing an Oxford Instruments EVO SEM and the Oxford Instruments Inca software. X-ray Photoelectron Spectroscopy (XPS) measurements were performed using a Kratos Axis HSi photoelectron spectrometer equipped with a charge neutralizer and a Mg Kα X-ray source ($h\nu$ = 1253.6 eV). Spectra were recorded at normal emission using an analyzer pass energy of 20 eV and X-ray power of 225 W. XRD patterns were recorded on a Panalytical X'pert-Pro diffractometer fitted with an X'celerator detector, using Cu Kα (1.54 Å) sources with a nickel filter, calibrated against Si standards. Raman spectra were obtained on a Renishaw Ramascope fitted with a 785 and 514 nm lasers. The spectra were recorded in the range of 0–1350 cm^{-1} using 514 nm source, 5× lens, 2 second exposure time, 100 accumulation and 100% laser power. Diffuse Reflectance Infra-red Fourier Transform (DRIFT) spectra were obtained using a Nicolet Avatar 370 MCT with Smart Collector accessory, mid/near infrared source and mercury cadmium telluride (MCT-A) photon detector at −196 °C (liquid N_2). Samples were diluted with KBr powder (10 wt% in KBr) for analysis then loaded into an environmental cell and subjected to additional drying under vacuum at 110 °C for 10 min prior to measurements to remove moisture physisorbed during air exposure. *Ex situ* pyridine adsorption was performed by exposure of samples to pyridine vapour in a desiccator overnight. Excess physisorbed pyridine was removed in a vacuum oven

prior to sample loading in the environmental cell, with spectra recorded at 25 °C *in vacuo*.

Acid site loadings were measured *via* NH_3 pulse chemisorption on a Quantachrome ChemBET 3000 system interfaced to an MKS Minilab mass spectrometer (MS). Samples were outgassed at 150 °C under flowing He (20 ml min^{-1}) for 2 h prior to pulse titration at 100 °C. The same procedure was employed to measure the base site loading, except that CO_2 was used to titrate sites at 35 °C. Acid strength measurements were made *via* flow adsorption calorimetry using a flow through differential scanning calorimeter (Setaram DSC111) connected to gas flow and switching systems. Gas flow rates were controlled by automated mass flow controllers. The sample (5–60 mg) was held on a glass frit in a vertical silica glass sample tube in the calorimeter. A steady 5 ml min^{-1} flow of He was maintained across the sample for 4 h at 150 °C to effect activation. A sequence of probe gas pulses (1% NH_3 in He) were delivered to the carrier gas stream from a 0.5 ml sample loop using a two position Valco valve with an automated micro-electric actuator. Heat output associated with interaction between NH_3 and sample was detected by DSC, and the concentration of NH_3 in the gas flow downstream of the DSC measured with a HPR 20 Hiden MS gas analyser *via* a heated capillary at 175 °C. A pulse delay (30 min) was employed to allow reversibly adsorbed NH_3 to desorb back into the pure He stream and/or redistribute on the sample, and for baselines to stabilise. pH measurements on aqueous catalyst suspensions were performed by adding 0.1 g of each catalyst to 20 ml of deionized water and stirring at room temperature. After 30 min the solution pH was measured using a Jenway 3305 pH meter.

Catalytic reactions

Initial kinetic studies of glucose and fructose conversion were conducted on a Radleys Starfish carousel under stirred batch conditions at 100 °C to facilitate detailed reaction profiling and minimise side reactions. Reactions were performed using 0.1 g glucose or fructose (Sigma Aldrich), 0.1 g SZ catalyst, and 20 ml deionised water, with such dilute sugar solutions selected deliberately to minimise side reactions of products. Samples were withdrawn periodically and filtered prior to analysis on an Agilent 1200 series HPLC equipped with RI and diode array detectors, and a Hi-Plex H column for analysis. A 5 mM aqueous solution of sulphuric acid was used as the eluent phase, with a flow rate of 0.6 ml min^{-1} and 65 °C column temperature. Product yields were calculated from response factors determined from multi-point calibration curves. Yields and selectivity were calculated on a carbon basis as below:

$$\text{HMF yield}[\%] = \frac{\text{Moles of carbon in HMF product}}{\text{Moles of carbon as glucose at } t = 0} \times 100$$

$$\text{HMF yield}[\%] = \frac{\text{Yield of HMF}}{\text{Glucose conversion}} \times 100$$

In some cases, due to the formation of humins and unidentified compounds, a 'relative selectivity' is used, to permit comparison of the reaction selectivity towards the following known and calibrated products: cellobiose, glucose, fructose, 1,6-anhydroglucose, lactic acid, formic acid, acetic acid, levulinic acid, HMF and furfural. Relative HMF selectivity is defined as:

$$\text{HMF relative selectivity}[\%] = \frac{\text{Yield of HMF}}{\text{Sum of yields of all identified products}} \times 100$$

Yield, selectivity and relative selectivity of other products are calculated on the same basis. Carbon balance is calculated based on moles of carbon in the identified products, relative to moles of carbon atoms in the glucose converted.

$$\frac{C_{out}}{C_{in}} = \frac{\sum(\text{Moles of } C \text{ in products})}{\text{Moles of } C \text{ in glucose converted}} \times 100$$

Results and discussion

Catalyst characterisation

Bifunctional SZ catalysts require surface sulfation of the $Zr(OH)_4$ precursor within the monolayer (ML) regime, and concomitant retention of a high accessible surface area. The impact of zirconium hydroxide impregnation by 0.01–0.5 M H_2SO_4 was probed by XPS and EDX to determine the SO_4 saturation monolayer coverage. Fig. 1 shows that increasing the concentration of the impregnating acid solution results in a steep initial rise in both the surface and bulk S content, which subsequently attain a plateau at ~5 and 3 wt% sulfur respectively. The transition between these regimes occurs at $[H_2SO_4] > 0.25$ M, indicative of a saturated sulfate monolayer. The surface S content is consistently higher than that of the bulk, confirming localisation of SO_4 species at the

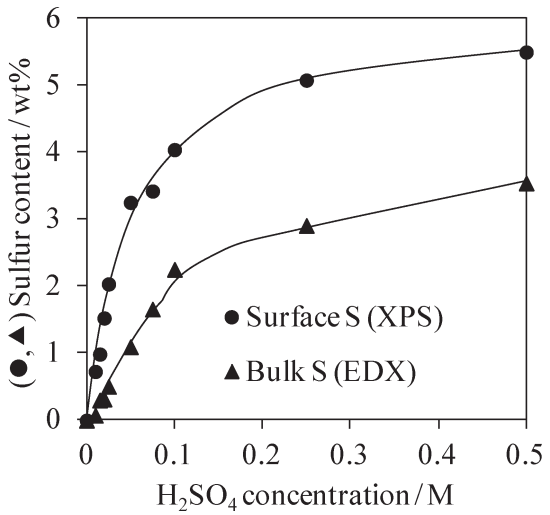

Fig. 1 Dependence of SZ surface and bulk sulfur content upon $[H_2SO_4]$.

$Zr(OH)_4$ surface. Defining the sulfate saturated monolayer point as 5 wt% S enables a sulfate calibration scale to be constructed for all SZ materials as implemented in Table S1.† SO_4 surface densities were calculated for comparison with literature, and are in good agreement with those of Morterra,[44] who determined a monolayer coverage of ~4 SO_4 per nm^{-2}. NH_3 titration and calorimetry revealed that increasing SO_4 coverage enhanced both the acid site loading and strength (Table 1) up to one monolayer.

Porosimetry (Fig. S1†) reveals all samples in the series exhibit a type IV isotherm with hysteresis loops indicative of bottle necked mesopores. Corresponding BET surface areas increase with SO_4 coverage up to the monolayer point (Table 1), with a subsequent decrease suggesting some structural collapse for the highest loading, *e.g.* formation of amorphous zirconium sulfate. Such surface area enhancements have been previously reported for SZ materials, wherein sulfation is reported to inhibit bulk crystallisation of the parent $Zr(OH)_4$ during calcination.[45] A shift in the hysteresis loop from P/P_0 = 0.6–0.8 to 0.4–0.6 with increasing S content reflects a decrease in the mean mesopore diameter in the BJH pore size distribution shown in Fig. S2,† which falls from 5 nm for the unsulfated calcined $Zr(OH)_4$ to 3.5 nm for samples impregnated with 0.01–0.025 M H_2SO_4. This mesoporosity likely arises from interparticle voids between sulfate functionalised ZrO_2 crystallites. Higher acid loadings induce additional microporosity, which we attribute to contraction of these interparticle voids as a result of more uniform crystallite packing as supported by XRD (see later), with $[H_2SO_4] > 0.5$ M eliminating this microporosity and suppressing mesoporosity, consistent with bulk sulfation.

The evolution of surface S species was probed *via* high resolution S 2p XP spectra (Fig. 2), which reveal a characteristic SO_4 peak between 168–172 eV for all SZ samples. In the low coverage regime ($\theta_{SO_4} < 0.5$ ML), this sulfate species shifts from 168.5 to 169 eV and broadens with increasing surface sulfation. These concomitant changes indicate the genesis of multiple, co-existing SO_4 species as surface sulfation progresses, likely associated with a change in coordination geometry from bidentate to monodentate[43] and diminishing charge withdrawal from the zirconia due to lateral interactions.

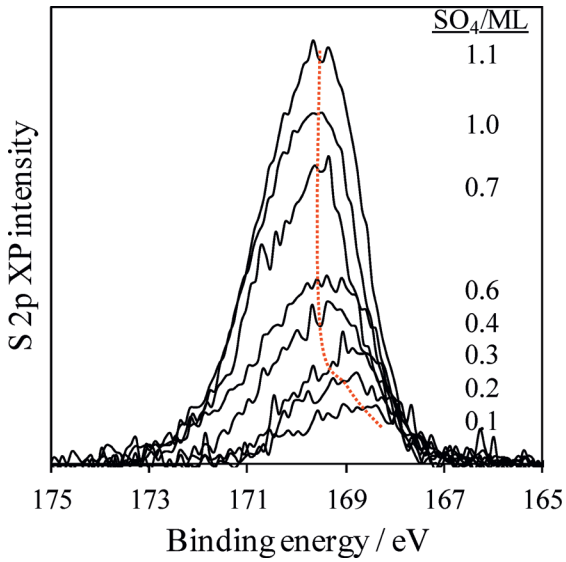

Fig. 2 S 2p XP spectra of sulfated $Zr(OH)_4$ as a function SO_4 coverage.

The presence of multiple SO_4^{2-} species is supported by DRIFTS measurements shown in Fig. 3, which show the progressive evolution of surface sulfoxy modes with increasing acid site loading. Vibrational bands are observed attributable to ν_s (S–O) at 1010, ν_{as} (S–O) at 1130, ν_s (S═O) at 1260 and ν_{as} (S═O) at 1362 cm^{-1}, consistent with bidentate or tridentate SO_4^{2-},[46–48] which grow monotonically with sulfate coverage up to 0.5 ML. The high ν_{as} (S═O) frequency indicates a highly covalent sulfate species, as reported by Morterra *et al.* for dehydrated samples measured *in vacuo*.[44,49] Peak broadening and poorer spectral resolution at higher coverage is attributable to the presence of multiple sulfate species as the monolayer is saturated.[14,15,50] The transition between isolated and polynuclear sulfate species is in good agreement with that reported by Bensitel[51] and Morterra[44] at SO_4 loadings >1.5 nm^{-2}.

The formation of crystalline species in calcined SZ samples was subsequently explored using powder XRD, Fig. 4. The sample with 0.1 ML SO_4 exhibited reflections arising from both monoclinic[10] (2θ = 24.7°, 28.4°, 31.6°) and tetragonal[11] (2θ = 30.3°, 35.3°, 50.7°, 59.9°, 60.6° and 63.5°) ZrO_2 phases. The tetragonal phase progressively increases with

Table 1 Physical properties of SZ as a function of SO_4 coverage

SO_4 coverage[a] /ML	Surface area[b] /m^2 g^{-1}	SO_4 density[c] /nm^{-2}	Acid loading[d] /mmol g^{-1}	$-\Delta H_{ads}$ (NH_3)[e] /kJ mol^{-1}
0.0	93	0	0.07	—
0.1	143	0.10	0.13	87
0.2	142	0.35	0.14	—
0.3	169	0.40	0.17	95
0.4	175	0.55	0.17	—
0.6	189	1.10	0.27	102
0.7	175	1.79	0.29	115
0.8	203	2.09	0.30	115
1.0	194	2.83	0.37	115
1.1	118	5.66	0.29	115

[a] Assuming 1 ML corresponds to 5 wt% surface S content. [b] From BET. [c] Using S content from EDX. [d] NH_3 TPD. [e] NH_3 adsorption calorimetry.

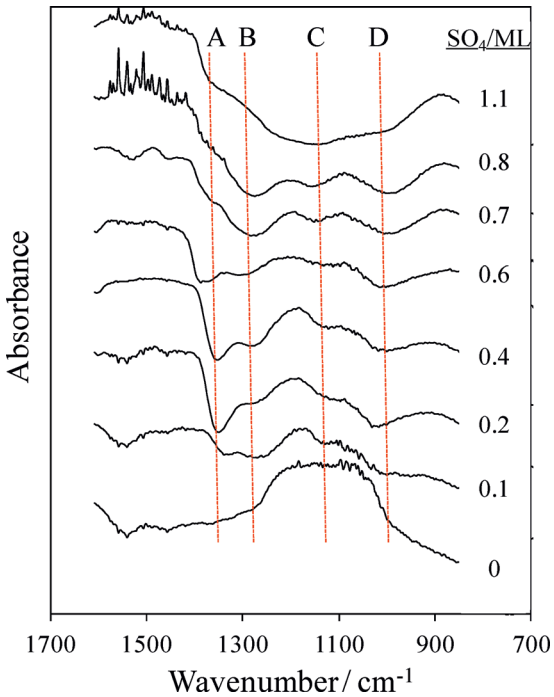

Fig. 3 DRIFTS spectra of impregnated sulphated zirconia as a function of bulk S content (spectra recorded *in situ* at 200 °C *in vacuo*).

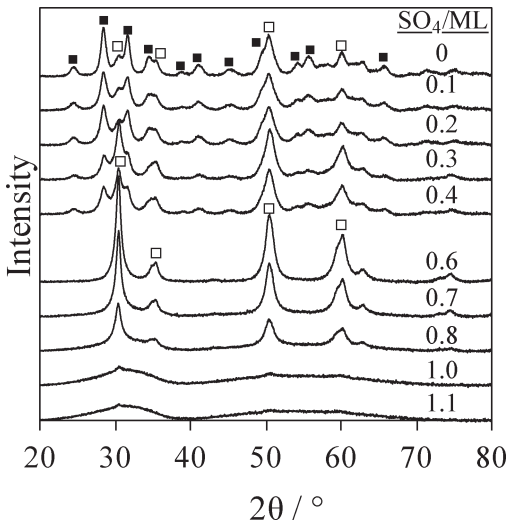

Fig. 4 Powder XRD analysis of impregnated sulphated zirconia catalysts showing the evolution of monoclinic (■) and tetragonal (□) phases as the bulk S content increases.

surface coverage, becoming the dominant phase for 0.75 ML SO_4^{2-}. A loss of crystallinity observed at higher S contents, is most likely due to the formation of an amorphous bulk $Zr(SO_4)_2$ species.[52]

Raman spectroscopy allows the clear discrimination of monoclinic and tetragonal phases of ZrO_2 (Fig. 5), and is in accordance with the powder XRD. Losses observed at 180, 307, 337, 381, 476 and 618 cm^{-1} for ZrO_2 are assigned to the monoclinic phase,[53] while bands evolving at 148, 271, 320,

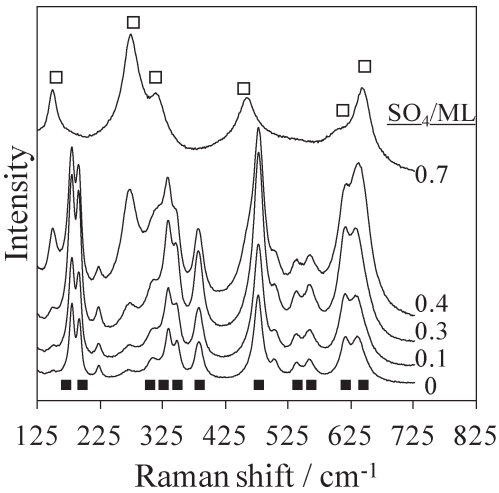

Fig. 5 Raman spectra of impregnated SZ catalysts showing the evolution of monoclinic (■) and tetragonal (□) phases with bulk S content.

456 and 645 cm^{-1} with increasing θ_{SO_4} are attributable to the tetragonal phase. High sulfate loadings degrade spectral resolution, resulting in poorer discrimination between the monoclinic and tetragonal modes as the monolayer point is reached, reflecting the surface sensitivity of Raman,[54] while new features emerge ~1000 cm^{-1} characteristic of surface sulphate species (Fig. S3†).

At low SO_4 loadings a single peak at 997 cm^{-1} is observed, with a second feature emerging at 1029 cm^{-1} which grows continuously above 0.2 ML to form a broad feature upon completion of the monolayer. This intense feature is attributed to the symmetric sulphate stretching mode, with peak-splitting suggesting a change in sulphate geometry. This transition in the Raman spectra occurs at θ_{SO_4} between 0.2 to 0.4 ML, precisely the point at which the tetragonal phase of ZrO_2 becomes stabilised. Hence we tentatively assign the 997 cm^{-1} and 1029 cm^{-1} Raman features to SO_4 coordinated to monoclinic and tetragonal surface sites respectively.

Zirconia is amphoteric, with the potential to exhibit Lewis basicity but also varying degrees of Lewis or Brønsted acidity depending on the crystalline phase, with monoclinic ZrO_2 generated *via* calcination reported to exhibit predominantly Lewis acidity.[55–57] The evolution of basic and Lewis–Brønsted acidic properties for the SZ materials was probed by CO_2 and NH_3 chemisorption and pyridine titration. The inset to Fig. 6 shows representative DRIFT spectra for pyridine adsorbed on submonolayer and monolayer SZ samples which exhibit bands at 1450, 1470, 1610 cm^{-1} attributed to pyridine bound to Lewis acid sites, while those at 1490, 1540, 1610 are 1635 cm^{-1} are characteristic of a pyridinium ion coordinate to Brønsted sites. The unique Brønsted–Lewis features at 1540/1450–1470 cm^{-1} were integrated to quantify the variation in Brønsted : Lewis ratio, which increases with both acid strength and SO_4 coverage (Fig. 6) and also correlates directly with the variation in tetragonal : monoclinic zirconia ratio (determined by integrating the

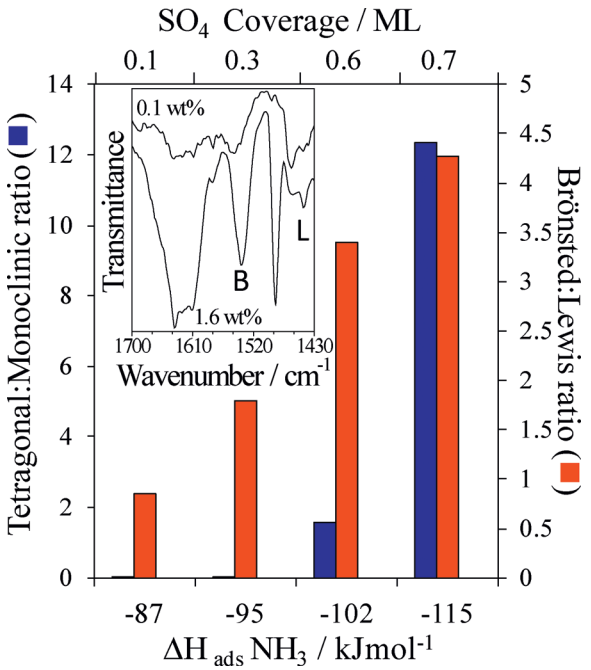

Fig. 6 Correlation between acid strength of SZ catalysts determined from calorimetry and evolution of Brønsted : Lewis ratio determined from pyridine titration (inset) and tetragonal : monoclinic ratios determined from Raman.

latter's fingerprint Raman bands at 270 and 380 cm^{-1} respectively from Fig. 5). These observations confirm that ZrO_2 morphology and acidity can be readily tuned by submonolayers of surface sulfate, consistent with previous reports that ZrO_2 crystallisation is dependent on surface sulfate density.[44] Calculations also show that ZrO_2 is also basic,[48] hence CO_2 titrations were employed to map the base site density as a function of sulfate loading. Fig. 7 shows that the calcined parent $Zr(OH)_4$, and submonolayer sulphated SZ materials, possess appreciable base site densities, albeit significantly lower than the corresponding acid site loadings (determined *via* NH_3 titration).

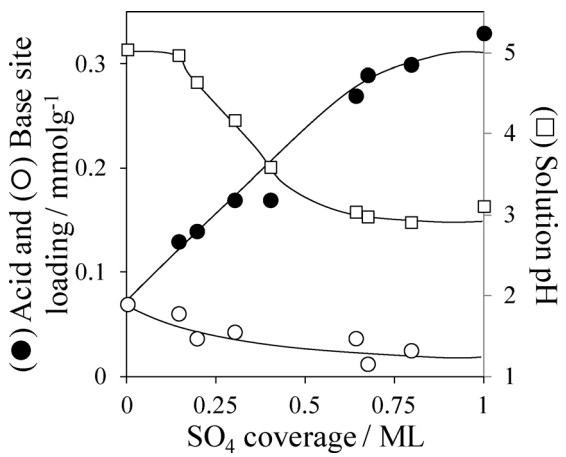

Fig. 7 Titration of acid and base site loadings of SZ catalysts as a function of S content.

The base site density decreases monotonically with increasing sulphate coverage, mirroring the fall in pH of aqueous suspensions of the SZ samples from pH 5 to 3, confirming that the balance of SZ acid–base character can be precisely tuned within the submonolayer regime ($\theta_{SO_4} < 1$).

The preceding holistic characterisation enables us to construct a model of the SZ system wherein a coverage-dependent transition occurs from isolated SO_4 species chemisorbed on monoclinic ZrO_2 → SO_4 islands on tetragonal and monoclinic ZrO_2 → a SO_4 monolayer bound to tetragonal ZrO_2.

Glucose conversion to 5-HMF

Glucose conversion to 5-HMF is proposed to initiate *via* a Lewis acid or base catalysed isomerisation to fructose, followed by a Brønsted acid catalysed dehydration as shown in Scheme 1. To establish the validity of this hypothesis, the kinetics of glucose *versus* fructose conversion to 5-HMF were compared at 100 °C. This mild temperature was employed to minimise competing degradation reactions to levulinic acid or humins, and thus permit accurate rate data to be obtained across the series of SZ materials.

Fig. 8 shows the resulting variations in glucose and fructose conversion as a function of surface sulfate coverage. The first striking observation is that whereas fructose conversion increases modestly with θ_{SO_4}, glucose conversion shows a large decrease for coverages above 0.25 ML. Glucose and fructose conversions and corresponding relative selectivities to the main dehydration products (5-HMF and furfural) are

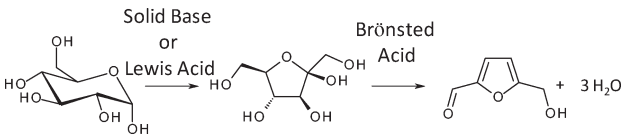

Scheme 1 Conversion of glucose to fructose and 5-HMF.

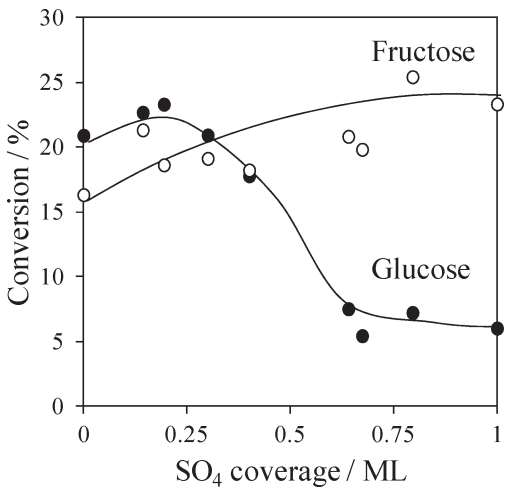

Fig. 8 Effect of SO_4 coverage on glucose and fructose conversion in water after 6 h reaction at 100 °C.

Table 2 Conversion and product selectivity following glucose and fructose dehydration over SO_4/ZrO_2 at 100 °C

SO_4 coverage/ML	Substrate	Conversion[a] /%	HMF[a] selectivity/%	Fructose[a] selectivity/%	Glucose[a] selectivity/%
0	Fructose	14.7	11.7	—	25.0
	Glucose	20.9	1.9	84.2	—
0.1	Fructose	16.2	13.3	—	26.4
	Glucose	22.7	3.0	81.3	—
0.2	Fructose	18.6	17.9	—	17.8
	Glucose	23.3 (42)	3.7 (11)	81.0 (71)	—
0.3	Fructose	19.1	19.9	—	16.2
	Glucose	20.9	4.8	78.2	—
0.4	Fructose	18.2	19.3	—	20.0
	Glucose	17.8	4.6	79.8	—
0.6	Fructose	20.8	29.9	—	8.1
	Glucose	7.5	10.5	63.9	—
0.7	Fructose	19.8	23.8	—	7.4
	Glucose	5.4	9.9	65.3	—
0.8	Fructose	25.4	32.6	—	8.1
	Glucose	7.2	10.0	77.2	—
1.0	Fructose	23.3	26.6	—	8.4
	Glucose	11.6 (37)	9.4 (18.5)	70.2 (41)	—
1.1	Fructose	16.6	28.2	—	9.0
	Glucose	5.5	7.7	81.5	—

[a] After 6 h reaction at 100 °C; remaining products are other sugar isomers and furfural (see Table S2). Values in brackets for 6 h reaction at 120 °C.

summarised in Table 2. While we note that 5-HMF yields are lower than those obtained in biphasic systems and ionic liquids, where 5-HMF yields as high as 60–70% are observed from glucose, it must be noted that these typically operate under higher temperature conditions of 120–200 °C and use homogeneous catalysts.[5] Indeed we find here that raising the reaction temperature to 120 °C almost doubles our conversion and triples our HMF selectivity for the most active catalyst. These trends can be rationalised in terms of the change in acid–base character with sulfur loading by comparing the associated product yields (Fig. 9). Glucose ↔ fructose isomerisation is a reversible reaction, catalysed by either basic or Lewis acid sites.

The high glucose conversion observed for pure ZrO_2 and SZ catalysts possessing low SO_4 coverages correlates with high fructose yields (Fig. 9a), and is thus a reflection of the correspondingly significant Lewis acid–base properties of these materials comprising predominantly monoclinic zirconia.

In contrast, high SO_4 coverages (*i.e.* Brønsted acid site densities) suppress glucose isomerisation to fructose in favour of HMF production associated with enhanced dehydration of the fructose intermediate. Hence loss of basicity and Lewis acidity upon zirconia sulfation switches off glucose ↔ fructose isomerisation but promotes the Brønsted acid catalysed fructose → 5-HMF pathway, in perfect agreement with the proposal in Scheme 1. The requirement for Brønsted acid character to produce 5-HMF is confirmed by inspecting the yield of products obtained from fructose as a substrate (Fig. 9b). Note that the resulting 5-HMF yields are three times higher starting from fructose *versus* glucose, indicating that glucose isomerisation to fructose is the rate-determining step in 5-HMF formation. TOFs for 5-HMF formation from fructose, normalised to the surface sulfate density, are independent of the Brønsted acid site loading/sulfur coverage and therefore acid strength, consistent with a common active acid site. SZ reactivity is thus predominantly controlled by the balance of their acid : base character; Fig. 10 shows a volcano

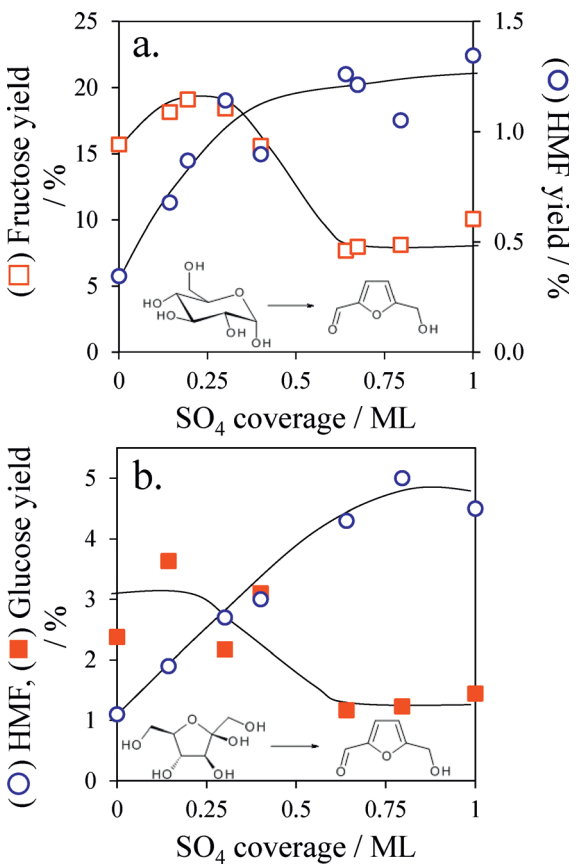

Fig. 9 Yields of a) fructose and 5-HMF during SZ catalysed glucose isomerisation and dehydration and b) glucose and 5-HMF during SZ catalysed fructose isomerisation after 6 h reaction at 100 °C.

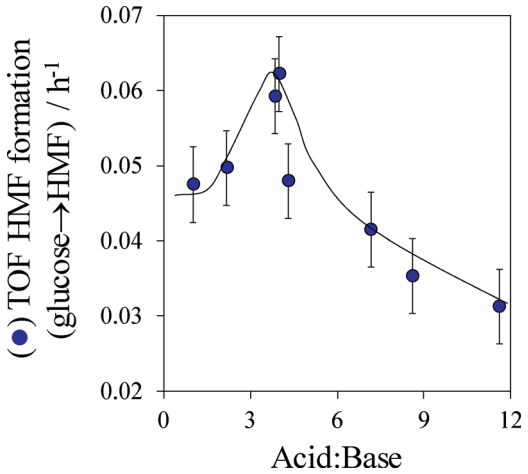

Fig. 10 Turnover frequencies for HMF formation from glucose at 100 °C as a function of acid : base ratio of SZ catalysts.

dependence for 5-HMF productivity, reflecting the requirement for both Lewis acidic–basic monoclinic ZrO_2 (to catalyse glucose isomerisation) and Brønsted surface sulfate species (to catalyse fructose dehydration to 5-HMF) in optimal catalyst formulations. Indeed the overall rate of 5-HMF production from glucose closely mirrors the mathematical product of the rate of glucose isomerisation with the rate of 5-HMF formed from direct fructose dehydration (Fig. S4†). To verify the stability of the optimum catalyst, a recycle test was performed following re-calcination of the spent catalyst at 550 °C, which revealed only a small decrease in absolute conversion was observed after 6 h reaction (Fig. S5†).

We can hence advance a bifunctional catalytic surface mechanism for glucose conversion to 5-HMF. The first step of this is most likely the Lewis base catalysed transformation of glucose into an enol intermediate (Scheme 2),[58,59] with subsequent protonation of the resulting C=C yielding either fructose or mannose. We propose that O^{2-} sites on the surface of base monoclinic ZrO_2 initiates this transformation *via* proton abstraction to form the enol (akin to that proposed over sodium aluminate[60]) which undergoes subsequent hydrogen transfer to form fructose. Spillover onto neighbouring Brønsted acid sulfate moieties then catalyses the stepwise dehydration of fructose to 5-HMF[61] as illustrated in Scheme 2. Lewis acid sites also have the potential to initiate glucose isomerisation *via* an intramolecular hydride shift.[62] However, the extent to which Lewis acid routes are able to participate in aqueous phase reactions remains contentious due to their likelihood of hydration to Brønsted counterparts, although it has been suggested that Lewis acidity may be retained at defect sites[44] or when hydrophobic supports such as Sn-β are employed[63] wherein a Meerwein–Ponndorf–Verley mechanism has been postulated.[64,65] As Fig. 10 highlights, careful tuning of the degree of zirconia surface sulfation enables the successful genesis of bi-functional catalysts possessing dual solid acid–base character which facilitate the telescopic conversion of glucose to 5-HMF under mild reaction conditions. To investigate the kinetics of the glucose → fructose → 5-HMF pathway dilute operating conditions using feed with only a 0.5 wt% (0.028 M) glucose concentration to minimize side reactions of 5-HMF. We note this is significantly lower than that reported in the literature, where typical concentrations range from 10 wt%,[28] 12 wt%[66] to 30 wt%.[67] However, it should be noted that for homogeneous processes, the conversion of glucose is reported to be exhibit good first order behaviour and is independent of concentration over the range 0.01–0.16 M.[68] Likewise, the kinetics of HMF formation from fructose are not reported to show a strong concentration dependence when operating at a fructose concentration ~0.7 M.[69] We thus expect that any changes in reactivity at higher initial glucose concentration would result in an increased probability of side reactions when more concentrated HMF containing mixtures are produced. In light of

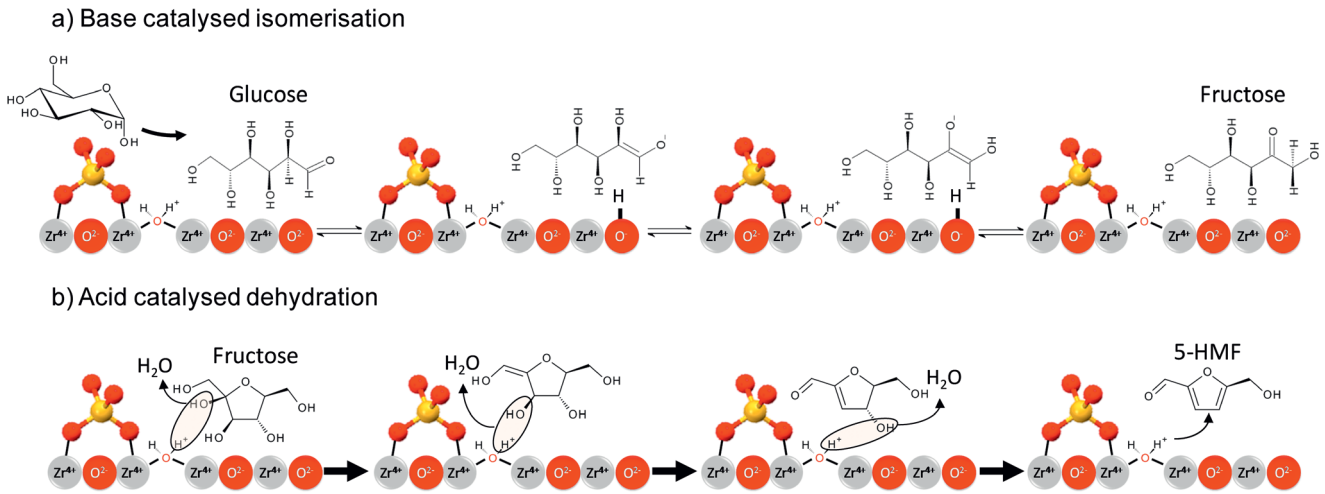

Scheme 2 Bi-functional surface catalysed mechanism for a) isomerisation of glucose to fructose over basic O^{2-} sites of monoclinic ZrO_2 (Lewis acidic Zr^{4+} may help stabilise the enolate intermediate) and b) dehydration of fructose to 5-HMF over Brønsted acid sites present in submonolayer SO_4/ZrO_2 catalysts.

this working at particularly high glucose concentrations may not be advisable and suggest operation in a biphasic system under more dilute glucose concentrations conditions could improve HMF selectivity under continuous processing conditions. We are presently investigating this and the synthesis of high area, nanoporous SZ analogues to afford even greater control over ZrO_2 crystallisation, and opportunities to tune catalyst hydrophobicity.

Conclusions

The impact of surface sulfation upon the physico-chemical properties of calcined $Zr(OH)_4$ has been systematically investigated by bulk and surface spectroscopies and chemical probes. The unsulfated precursor forms predominantly monoclinic zirconia possessing mixed Lewis acid and base surface sites and is effective for glucose isomerisation to fructose but poor towards fructose dehydration to 5-HMF. Dilute sulfuric acid pre-treatment of $Zr(OH)_4$ and subsequent calcination results exclusively in the formation of polydentate surface SO_4^{2-} species, and concomitant stabilisation of tetragonal ZrO_2, conferring significant Brønsted acidity and corresponding enhanced 5-HMF production from either glucose or fructose. Higher degrees of surface sulfation ($\theta_{SO_4} >$ 0.25 ML), and attendant loss of surface basicity from exposed zirconia, progressively switches off glucose ↔ fructose isomerisation, while continuing to promote fructose → 5-HMF. Saturated sulfate monolayers present a distribution of mono and polynuclear sulfate species chemisorbed over tetragonal crystalline zirconia and/or amorphous zirconium sulfate, and the resulting materials (which exhibit almost entirely Brønsted acid character) are the least efficient for 5-HMF synthesis from glucose. Submonolayer sulfate coverages of approximately 0.3 ML afford the optimal mix of Lewis base sites arising from accessible ZrO_2, and co-existing Brønsted acid sites arising from mono- or bidentate sulfate, required for the tandem isomerisation of glucose to fructose and the latter's subsequent dehydration to 5-HMF. The design of such bi-functional catalysts capable of effecting one-pot telescopic syntheses in aqueous media will become increasingly critical to achieve atom-economical, selective transformations of bio-derived molecules for sustainable chemicals and fuels.

Acknowledgements

We thank the EPSRC for funding under (EP/K000616/1) and MEL Chemicals for the supply of $Zr(OH)_4$. KW acknowledges The Royal Society for the award of an Industry Fellowship, and AFL thanks the EPSRC for the award of a Leadership Fellowship (EP/G007594/2). Financial support from the Spanish Ministry of Economy and Competitiveness through the project CTQ2011-28216-C02-01 is also kindly acknowledged. This Article is published in celebration of the 50th Anniversary of the opening of the Chemistry Department at the University of York.

Notes and references

1 M. J. Climent, A. Corma and S. Iborra, *Green Chem.*, 2011, **13**, 520–540.
2 P. Gallezot, *Chem. Soc. Rev.*, 2012, **41**, 1538–1558.
3 T. Werpy and G. Petersen, Top Added Chemicals from Biomass Volume 1—Results of Screening for Potential Candidates from Sugars and Synthesis Gas, U. S. Department of Energy Report, 2004.
4 J. J. Bozell and G. R. Petersen, *Green Chem.*, 2010, **12**, 539–554.
5 R.-J. van Putten, J. C. van der Waal, E. de Jong, C. B. Rasrendra, H. J. Heeres and J. G. de Vries, *Chem. Rev.*, 2013, **113**, 1499–1597.
6 A. Corma, S. Iborra and A. Velty, *Chem. Rev.*, 2007, **107**, 2411–2502.
7 B. F. M. Kuster, *Starch/Staerke*, 1990, **42**, 314–321.
8 Y. Roman-Leshkov, J. N. Chheda and J. A. Dumesic, *Science*, 2006, **312**, 1933–1937.
9 Y. Zhang, J. Wang, J. Ren, X. Liu, X. Li, Y. Xia, G. Lu and Y. Wang, *Catal. Sci. Technol.*, 2012, **2**, 2485–2491.
10 J. Wang, W. Xu, J. Ren, X. Liu, G. Lu and Y. Wang, *Green Chem.*, 2011, **13**, 2678–2681.
11 Q. Cao, X. Guo, J. Guan, X. Mu and D. Zhang, *Appl. Catal., A*, 2011, **403**, 98–103.
12 Q. Zhao, L. Wang, S. Zhao, X. Wang and S. Wang, *Fuel*, 2011, **90**, 2289–2293.
13 C. Carlini, P. Patrono, A. M. R. Galletti and G. Sbrana, *Appl. Catal., A*, 2004, **275**, 111–118.
14 A. J. Crisci, M. H. Tucker, J. A. Dumesic and S. L. Scott, *Top. Catal.*, 2010, **53**, 1185–1192.
15 P. Carniti, A. Gervasini and M. Marzo, *Catal. Commun.*, 2011, **12**, 1122–1126.
16 X. H. Qi, M. Watanabe, T. M. Aida and R. L. Smith, *Catal. Commun.*, 2009, **10**, 1771–1775.
17 P. Carniti, A. Gervasini, S. Biella and A. Auroux, *Catal. Today*, 2006, **118**, 373–378.
18 X. H. Qi, H. X. Guo and L. Y. Li, *Ind. Eng. Chem. Res.*, 2011, **50**, 7985–7989.
19 H. E. Van Dam, A. P. G. Kieboom and H. Van Bekkum, *Starch/Staerke*, 1986, **38**, 95–101.
20 Y. Nakamura and S. Morikawa, *Bull. Chem. Soc. Jpn.*, 1980, **53**, 3705–3706.
21 C. Moreau, M. N. Belgacem and A. Gandini, *Top. Catal.*, 2004, **27**, 11–30.
22 H. B. Zhao, J. E. Holladay, H. Brown and Z. C. Zhang, *Science*, 2007, **316**, 1597–1600.
23 W. G. Glasser and R. S. Wright, *Biomass Bioenergy*, 1998, **14**, 219–235.
24 P. Alvira, E. Tomás-Pejó, M. Ballesteros and M. J. Negro, *Bioresour. Technol.*, 2010, **101**, 4851–4861.
25 W. S. Mok, M. J. Antal and G. Varhegyi, *Ind. Eng. Chem. Res.*, 1992, **31**, 94–100.
26 R. Rinaldi and F. Schüth, *ChemSusChem*, 2009, **2**, 1096–1107.
27 C. V. McNeff, D. T. Nowlan, L. C. McNeff, B. W. Yan and R. L. Fedie, *Appl. Catal., A*, 2010, **384**, 65–69.

28 J. N. Chheda, Y. Roman-Leshkov and J. A. Dumesic, *Green Chem.*, 2007, **9**, 342–350.
29 Y. J. Pagan-Torres, T. Wang, J. M. R. Gallo, B. H. Shanks and J. A. Dumesic, *ACS Catal.*, 2012, **2**, 930–934.
30 V. V. Ordomsky, J. van der Schaaf, J. C. Schouten and T. A. Nijhuis, *J. Catal.*, 2012, **287**, 68–75.
31 C. Moreau, R. Durand, S. Razigade, J. Duhamet, P. Faugeras, P. Rivalier, P. Ros and G. Avignon, *Appl. Catal., A*, 1996, **145**, 211–224.
32 P. Rivalier, J. Duhamet, C. Moreau and R. Durand, *Catal. Today*, 1995, **24**, 165–171.
33 Y. J. Pagan-Torres, T. F. Wang, J. M. R. Gallo, B. H. Shanks and J. A. Dumesic, *ACS Catal.*, 2012, **2**, 930–934.
34 V. Choudhary, S. H. Mushrif, C. Ho, A. Anderko, V. Nikolakis, N. S. Marinkovic, A. I. Frenkel, S. I. Sandler and D. G. Vlachos, *J. Am. Chem. Soc.*, 2013, **135**, 3997–4006.
35 C. B. Rasrendra, I. G. B. N. Makertihartha, S. Adisasmito and H. J. Heeres, *Top. Catal.*, 2010, **53**, 1241–1247.
36 T. F. Wang, Y. J. Pagan-Torres, E. J. Combs, J. A. Dumesic and B. H. Shanks, *Top. Catal.*, 2012, **55**, 657–662.
37 E. Nikolla, Y. Roman-Leshkov, M. Moliner and M. E. Davis, *ACS Catal.*, 2011, **1**, 408–410.
38 A. Takagaki, M. Ohara, S. Nishimura and K. Ebitan, *Chem. Commun.*, 2009, 6276–6278.
39 M. A. Aramendıa, V. Boráu, C. Jiménez, J. M. Marinas, A. Marinas, A. Porras and F. J. Urbano, *J. Catal.*, 1999, **183**, 240–250.
40 K. Tanabe and T. Yamaguchi, *Catal. Today*, 1994, **20**, 185–197.
41 X. Qi, M. Watanabe, T. M. Aida and R. L. Smith Jr., *Catal. Commun.*, 2008, **9**, 2244–2249.
42 I. J. Dijs, J. W. Geus and L. W. Jenneskens, *J. Phys. Chem. B*, 2003, **107**, 13403–13413.
43 M. A. Ecormier, K. Wilson and A. F. Lee, *J. Catal.*, 2003, **215**, 57–65.
44 C. Morterra, G. Cerrato, C. Emanuel and V. Bolis, *J. Catal.*, 1993, **142**, 349–367.
45 G. D. Yadav and J. J. Nair, *Microporous Mesoporous Mater.*, 1999, **33**, 1–48.
46 K. Nakamoto, J. Fujita, S. Tanaka and M. Kobayashi, *J. Am. Chem. Soc.*, 1957, **79**, 4904–4908.
47 S. J. Hug, *J. Colloid Interface Sci.*, 1997, **188**, 415–422.
48 F. Haase and J. Sauer, *J. Am. Chem. Soc.*, 1998, **120**, 13503–13512.
49 C. Morterra, G. Cerrato, F. Pinna, M. Signoretto and G. Strukul, *J. Catal.*, 1994, **149**, 181.
50 T. Yamaguchi, T. Jin and K. Tanabe, *J. Phys. Chem. B*, 1986, **90**, 3148–3152.
51 M. Bensitel, O. Saur, J. C. Lavalley and B. A. Morrow, *Mater. Chem. Phys.*, 1988, **19**, 147–156.
52 J. R. Sohn, T. D. Kwon and S. B. Kim, *J. Korean Chem. Soc.*, 2001, **22**, 1309–1315.
53 D. I. Torres and J. Llopis, *Superlattices Microstruct.*, 2009, **45**, 482–488.
54 M. Li, Z. Feng, G. Xiong, P. Ying, Q. Xin and C. Li, *J. Phys. Chem. B*, 2001, **105**, 8107–8111.
55 V. Bolis, C. Morterra, M. Volante, L. Orio and B. Fubini, *Langmuir*, 1990, **6**, 695–701.
56 V. Bolis, G. Cerrato, G. Magnacca and C. Morterra, *Thermochim. Acta*, 1998, **312**, 63–77.
57 W. Hertl, *Langmuir*, 1989, **5**, 96–100.
58 D. W. Harris and M. S. Feather, *J. Am. Chem. Soc.*, 1975, **97**, 178–181.
59 H. S. Isbell, H. L. Frush, C. W. R. Wade and C. E. Hunter, *Carbohydr. Res.*, 1969, **9**, 163–175.
60 A. J. Shaw Iii and G. T. Tsao, *Carbohydr. Res.*, 1978, **60**, 327–325.
61 M. J. Antal Jr., W. S. L. Mok and G. N. Richards, *Carbohydr. Res.*, 1990, **199**, 91–109.
62 Y. Román-Leshkov, M. Moliner, J. A. Labinger and M. E. Davis, *Angew. Chem., Int. Ed.*, 2010, **49**, 8954–8957.
63 M. Moliner, Y. Román-Leshkov and M. E. Davis, *Proc. Natl. Acad. Sci. U. S. A.*, 2010, **107**, 6164–6168.
64 J. F. Miñambres, M. A. Aramendía, A. Marinas, J. M. Marinas and F. J. Urbano, *J. Mol. Catal. A: Chem.*, 2011, **338**, 121–129.
65 F. J. Urbano, M. A. Aramendía, A. Marinas and J. M. Marinas, *J. Catal.*, 2009, **268**, 79–88.
66 K. Lourvanij and G. L. Rorrer, *Ind. Eng. Chem. Res.*, 1993, **32**, 11–19.
67 A. Ranoux, K. Djanashvili, I. W. C. E. Arends and U. Hanefeld, *ACS Catal.*, 2013, **3**, 760–763.
68 B. M. Kabyemela, T. Adschiri, R. M. Malaluan and K. Arai, *Ind. Eng. Chem. Res.*, 1997, **36**, 1552–1558.
69 G. R. Akien, L. Qi and I. T. Horvath, *Chem. Commun.*, 2012, **48**, 5850–5852.

